

Parametrizing surface wave tomographic models with harmonic spherical splines

Abel Amirbekyan,^{1,*} Volker Michel¹ and Frederik J. Simons^{2,†}

¹Geomathematics Group, Department of Mathematics, University of Kaiserslautern, PO Box 3049, 67653 Kaiserslautern, Germany

²Department of Geosciences, Princeton University, Guyot Hall, Princeton, NJ 08544, USA. E-mail: fjsimons@alum.mit.edu

Accepted 2008 April 1. Received 2008 April 1; in original form 2007 August 31

SUMMARY

We present a mathematical framework and a new methodology for the parametrization of surface wave phase-speed models, based on traveltimes data. Our method is neither purely local, like block-based approaches, nor is it purely global, like those based on spherical harmonic basis functions. Rather, it combines the well-known theory and practical utility of the spherical harmonics with the spatial localization properties of spline basis functions. We derive the theoretical foundations for the application of harmonic spherical splines to surface wave tomography and summarize the results of numerous numerical tests illustrating the performance of a practical inversion scheme based upon them. Our presentation is based on the notion of reproducing-kernel Hilbert spaces, which lends itself to the parametrization of fully 3-D tomographic earth models that include body waves as well.

Key words: Numerical approximation and analysis; Fourier analysis; Inverse theory; Tomography; Seismic tomography; Surface waves and free oscillations.

1 INTRODUCTION

Surface wave tomography, which we define here to be the inverse problem that solves for lateral inhomogeneities in the phase speed of seismic surface waves, given measurements, made in a specific period range, of their traveltimes from a collection of earthquake sources to a set of seismometers (see, e.g. Nolet 1987), may be represented mathematically by the integral equation

$$\int_{\gamma_q} c^{-1}(\hat{\mathbf{f}}) d\gamma = t_q \quad \text{for } q = 1, \dots, N, \quad (1)$$

where c^{-1} is the desired phase ‘slowness’ at the geographical location $\hat{\mathbf{f}}$ on the Earth’s surface, the curve γ_q is the surface ray path from the epicentre to the recording station and $d\gamma$ its differential angular arc length, and t_q the corresponding traveltime datum. It is to be noted that the paths γ_q themselves depend on the unknown phase-speed distribution, thereby rendering the tomographic inverse problem intrinsically non-linear. Keeping with common seismological practice, however, here we focus on the linearized version of this problem, in which the seismic ray path is a geodesic minimal arc, or great-circle path, that connects epicentre and station. This approximation is generally valid when the wave speeds vary only slightly, and smoothly, from spherically symmetric background models such

as the Preliminary Reference Earth Model (Dziewoński & Anderson 1981). In this sense, seismologists usually deal with traveltime ‘anomalies’, the difference between the traveltimes that are observed and those predicted from the reference model and solve for local wave speed ‘perturbations’ in the sense $\delta c(\hat{\mathbf{f}})/c_R$, where c_R is the reference phase speed. Neither this fact nor the fact that eq. (1) is an infinite-frequency, ray-theoretical approximation, which, though it has been the dominant approach historically, is currently undergoing a paradigm shift (e.g. Dahlen *et al.* 2000; Hung *et al.* 2000; Zhou *et al.* 2004; Nissen-Meyer *et al.* 2007), fundamentally change the results presented in this paper.

Knowledge of how seismic wave speeds vary throughout the Earth is an important research goal (e.g. Romanowicz 2003, 2008). Although this ultimately motivates our study, here we limit ourselves to reporting on a mathematical advance in the methodology of seismic surface wave tomography, rather than on obtaining and interpreting results relevant to the geological sciences *per se*. Our present contribution concerns the representation and retrieval of the solution space of the wave speed pattern $c(\hat{\mathbf{f}})$ in eq. (1), which we refer to as the ‘earth model’.

Tomographic studies—and this not only in seismology—usually parametrize the target model by local or global basis functions (Nolet 2008). The former may take the form of a set of non-overlapping (and not necessarily regularly spaced) blocks, cells, nodes or voxels (e.g. Aki *et al.* 1977; Zhang & Tanimoto 1993; Spakman & Bijwaard 2001; Simons *et al.* 2002; Debayle & Sambridge 2004; Nolet & Montelli 2005) that serve as strictly local characteristic functions; they may be smooth, spatially localized, functions such as cubic B-splines (e.g. Wang & Dahlen 1995; Wang *et al.* 1998; Boschi *et al.* 2004); or wavelets (e.g. Chiao & Kuo 2001; Chevrot &

*Now at: The Fraunhofer-Institut für Techno-und Wirtschaftsmathematik ITWM, Fraunhofer-Platz 1, 67663 Kaiserslautern, Germany.

†Previously at: Department of Earth Sciences, University College London, Gower Street, London WC1E 6BT, UK.

Zhao 2007; Loris *et al.* 2007). The latter most commonly are spherical harmonics (e.g. Dziewoński 1984; Woodhouse & Dziewoński 1984; Ekström *et al.* 1997; Trampert & Woodhouse 1996, 2001), whose support is, by definition, global (Freeden & Michel 1999); in this case, and for this reason, additional damping and smoothness criteria are often imposed on the solution (Boschi & Dziewoński 1999).

Inversion strategies that don't, properly speaking, parametrize the model exist (e.g. Backus & Gilbert 1970; Tarantola & Valette 1982), but then, these usually rely on the prescription of a very specific resolution criterion in the 'Backus–Gilbert' approach (e.g. Backus & Gilbert 1968), or of *a priori*, that is, parametrized, forms of the model covariance matrix in the 'Bayesian' approach (e.g. Tarantola & Necessian 1984; Montagner 1986). And, of course, even in those cases, discretization of the model remains necessary for its representation.

Model decompositions based on spherical harmonics have many advantages. The mathematical properties of spherical harmonics have long been studied intensively (e.g. Byerly 1893), and a multitude of numerical tools are available for application in seismic tomography (e.g. Doornbos 1988; Dahlen & Tromp 1998). Furthermore, the results of seismic tomographic inversions are often interpreted in a geodynamic context by comparing them to the (predicted) behaviour of the gravitational or magnetic anomaly fields of the Earth, themselves handily expressed in the spherical harmonic basis (e.g. Hager *et al.* 1985; Forte *et al.* 1995; Pari & Peltier 1996). Last, the regularization of the commonly ill-posed tomographic inverse problem, which has a somewhat *ad hoc* character with strictly local parametrizations, retains the intuitive quality of an isotropic low-pass filtering operation in the spherical harmonic basis (see, e.g. Boschi & Dziewoński 1999), which is both easily implemented and readily assessable.

One evident drawback of spherical harmonics is their global character. Since seismic events mostly originate in narrow regions of plate boundary activity and the distribution of seismic stations varies extremely over the planet—that is, until the oceans are covered with recording units (Simons *et al.* 2006b), the available seismic coverage is far from uniform. Due to this, the interior structure of the Earth can only be coarsely resolved in some areas, though more detailed models can be obtained elsewhere. An unwanted result of using global basis functions is that spurious structure may 'leak' into the underresolved portions of the model (Boschi & Dziewoński 1999). Another drawback is the necessarily truncated representation of the model by a finite set of spherical harmonic basis functions, which introduces a second source of leakage into the solution. Both spatial inhomogeneity or incompleteness of sampling and spectral model bandlimitation effect to bias the solution to the inverse problem away from the truth; such problems and some of their possible solutions are discussed in more detail in different contexts by Trampert & Snieder (1996) and Simons & Dahlen (2006).

The above discussion is not meant to deny that ultimately, the physics of the forward problem, rather than sheer mathematical convenience, should have a hand in deciding on a suitable parametrization. We sidestep this issue by focusing on surface wave models of wave speed, for which the spherical harmonics undeniably are a natural as well as convenient choice.

Here, we outline an approach that preserves the desirable analytical properties of spherical harmonic based tomographic parametrization while enabling the retrieval of localized information and avoiding the mapping of well-resolved areas into the unconstrained parts of the solution. The basis functions we propose to use in this context are the harmonic spherical splines of Freeden

(1981a,b). These are, as we shall recall, constructed via spatially localizing reproducing kernels (Freeden *et al.* 1998; Freeden & Michel 2004) and have previously been applied successfully in geoscientific applications such as the analysis of gravity data (e.g. Fengler *et al.* 2004), modelling of the density distribution inside the Earth (e.g. Michel 1999; Fengler *et al.* 2006; Michel & Wolf 2008), modelling of seismic wave front propagation (e.g. Kammann & Michel 2008) and deformation analysis (e.g. Tücks 1996). Many of the ideas share intimate connections with or go back to work done in geomagnetism (e.g. Whaler & Gubbins 1981; Shure *et al.* 1982; Parker 1994) and ultimately, as ever often the case, to Backus & Gilbert (1968, 1970) and Backus (1970a,b,c). Finally, we note that Yanovskaya & Ditmar (1990) have drawn some of the most insightful parallels between smoothed parametrized, Backus–Gilbert, and Bayesian inversion strategies in the specific context of surface wave tomography.

Here, we derive the theoretical foundations for the application of harmonic spherical splines to the problem of surface wave tomography and present the results of numerical tests justifying our enthusiasm for this new method.

2 HARMONIC SPLINES ON THE SPHERE

In this section we present a concise introduction to the theory of spherical splines based on reproducing-kernel Hilbert spaces. We refer the reader to the literature for further mathematical details and proofs (e.g. Aronszajn 1950; Freeden 1981a,b; Schreiner 1997a; Freeden *et al.* 1998; Freeden 1999) and to Parker (1994) for a lucid, geophysically oriented treatment of the main concepts.

2.1 Spherical harmonics

We begin with a brief exposé about spherical harmonics, referring the reader elsewhere for further mathematical (e.g. Müller 1966; Freeden *et al.* 1998) or geophysical (e.g. Kellogg 1967; Backus *et al.* 1996; Dahlen & Tromp 1998) details. We denote as \mathbb{N}_0 the set of all positive integers including 0 and use \mathbb{R} for the set of all real numbers. The standard Euclidian inner product on \mathbb{R}^3 is denoted by $\mathbf{x} \cdot \mathbf{y} := \sum_{i=1}^3 x_i y_i$ and the Euclidian norm is written $\|\mathbf{x}\| := (\mathbf{x} \cdot \mathbf{x})^{1/2}$. The unit sphere $\Omega := \{\hat{\mathbf{r}} \in \mathbb{R}^3 : \|\hat{\mathbf{r}}\| = 1\}$ is taken to be a reasonable approximation to the Earth's surface. The set of real surface spherical harmonics $\{Y_{lm}(\hat{\mathbf{r}})\}_{m=-l, \dots, l}$ of integer degree l and order m spans the space of harmonic homogeneous polynomials of degree l restricted to the unit sphere Ω . The set $\{Y_{lm}\}_{l \in \mathbb{N}_0; m=-l, \dots, l}$ forms a complete orthonormal system in the space of square-integrable functions confined to the unit sphere. This space, $\mathcal{L}^2(\Omega)$ or \mathcal{L}^2 for short, is equipped with the inner product

$$\langle Y_{lm}, Y_{l'm'} \rangle_{\mathcal{L}^2} := \int_{\Omega} Y_{lm}(\hat{\mathbf{r}}) Y_{l'm'}(\hat{\mathbf{r}}) d\Omega = \delta_{ll'} \delta_{mm'}, \quad (2)$$

where δ is the Kronecker delta. The spherical harmonics satisfy the addition theorem

$$\sum_{m=-l}^l Y_{lm}(\hat{\mathbf{r}}) Y_{lm}(\hat{\mathbf{r}}') = \left(\frac{2l+1}{4\pi} \right) P_l(\hat{\mathbf{r}} \cdot \hat{\mathbf{r}}'), \quad (3)$$

where P_l is the Legendre polynomial of degree l and $\hat{\mathbf{r}} \cdot \hat{\mathbf{r}}' = \cos \Delta$, with Δ being the geodesic angular distance between the points $\hat{\mathbf{r}}$ and $\hat{\mathbf{r}}'$. Expressions of type (3) only depend on the angular distance between two points on a sphere and are therefore termed 'radial basis functions'.

The real surface harmonics Y_{lm} that we use in this paper relate to the perhaps more widely used complex harmonics \mathcal{Y}_{lm} as

$$Y_{lm} = \begin{cases} \sqrt{2} \operatorname{Re} \mathcal{Y}_{|m|} & \text{if } -l \leq m < 0 \\ \mathcal{Y}_{lm} & \text{if } m = 0 \\ \sqrt{2} \operatorname{Im} \mathcal{Y}_{lm} & \text{if } 0 < m \leq l, \end{cases} \quad (4)$$

whereby for colatitude θ and longitude ϕ (Edmonds 1996)

$$\mathcal{Y}_{lm}(\theta, \phi) = X_{lm}(\theta) \exp(im\phi), \quad (5)$$

$$X_{lm}(\theta) = (-1)^m \left(\frac{2l+1}{4\pi} \right)^{1/2} \left[\frac{(l-m)!}{(l+m)!} \right]^{1/2} P_{lm}(\cos\theta), \quad (6)$$

$$P_{lm}(\mu) = \frac{1}{2^l l!} (1 - \mu^2)^{m/2} \left(\frac{d}{d\mu} \right)^{l+m} (\mu^2 - 1)^l. \quad (7)$$

2.2 Reproducing-kernel Hilbert spaces

With a sequence of non-zero real numbers $\{A_l\}_{l \in \mathbb{N}_0}$ such that

$$\sum_{l=0}^{\infty} \left(\frac{2l+1}{4\pi} \right) A_l^{-2} < \infty, \quad (8)$$

we associate a space, $\mathcal{H}(\Omega)$ or \mathcal{H} for short, that contains all $f, g \in \mathcal{L}^2(\Omega)$ functions, with finite inner product

$$\langle f, g \rangle_{\mathcal{H}} := \sum_{l=0}^{\infty} \sum_{m=-l}^l A_l^2 \langle f, Y_{lm} \rangle_{\mathcal{L}^2} \langle g, Y_{lm} \rangle_{\mathcal{L}^2} < \infty, \quad (9)$$

and norm $\|f\|_{\mathcal{H}} := \langle f, f \rangle_{\mathcal{H}}^{1/2}$. The summability (8) implies that every function in \mathcal{H} is continuous on Ω (Freeden 1999). Such a space \mathcal{H} possesses a unique ‘reproducing kernel’ $K_{\mathcal{H}} : \Omega \times \Omega \rightarrow \mathbb{R}$,

$$K_{\mathcal{H}}(\hat{\mathbf{r}}, \hat{\mathbf{r}}') = \sum_{l=0}^{\infty} \sum_{m=-l}^l A_l^{-2} Y_{lm}(\hat{\mathbf{r}}) Y_{lm}(\hat{\mathbf{r}}') \quad (10)$$

$$= \sum_{l=0}^{\infty} A_l^{-2} \left(\frac{2l+1}{4\pi} \right) P_l(\hat{\mathbf{r}} \cdot \hat{\mathbf{r}}'), \quad (11)$$

which, writing ‘ \cdot ’ for the function’s argument to which the inner product is applied, implies the properties

$$K_{\mathcal{H}}(\hat{\mathbf{r}}, \cdot), K_{\mathcal{H}}(\cdot, \hat{\mathbf{r}}) \in \mathcal{H}, \quad (12a)$$

$$\langle f, K_{\mathcal{H}}(\hat{\mathbf{r}}, \cdot) \rangle_{\mathcal{H}} = \langle f, K_{\mathcal{H}}(\cdot, \hat{\mathbf{r}}) \rangle_{\mathcal{H}} = f(\hat{\mathbf{r}}), \quad (12b)$$

for all $f \in \mathcal{H}$ and $\hat{\mathbf{r}} \in \Omega$. Thus, the inner product of a function in the particular space \mathcal{H} and the kernel $K_{\mathcal{H}}$ ‘reproduces’ the function.

Reproducing-kernel Hilbert spaces are usually thought of as containing ‘smooth’ functions, and the quelling sequence $\{A_l\}_{l \in \mathbb{N}_0}$, while arbitrary in principle, can be chosen judiciously to yield ‘interesting’ or ‘convenient’ reproducing kernels (e.g. Schreiner 1997a; Freedon *et al.* 1998; Freedon & Michel 1999), or they may be dictated by the physics of the problem at hand (e.g. Shure *et al.* 1982; Parker 1994). Choices abound; the basic idea relevant to our discussion is that the decay of A_l^{-2} determines the spatio-spectral localization properties of the reproducing kernel. To take a non-bandlimited example, if $A_l = 1$, eqs (10) and (11) merely define the spherical Dirac delta function, which has infinite localization in space but contains all frequencies. If $A_l = 1$ only up to a certain bandwidth $l \leq L$, the

resulting ‘Shannon’ kernel has both space and spectral localization (see also Simons *et al.* 2006a). Finally, at the other extreme, if $A_l = \delta_{ll'}$, we obtain the spherical harmonics of degree l —ideally localized spectrally but completely unlocalized in space.

Fig. 1 shows an intermediate case, the so-called ‘Abel–Poisson’ kernel, defined by eq. (10), with the sequence or ‘symbol’,

$$A_l = h^{-l/2} \quad \text{for } 0 < h < 1. \quad (13)$$

The Abel–Poisson kernel has the remarkable closed-form expression (Freedon & Schreiner 1995)

$$K_{\mathcal{H}}(\hat{\mathbf{r}}, \hat{\mathbf{r}}') = \frac{1 - h^2}{4\pi(1 + h^2 - 2h[\hat{\mathbf{r}} \cdot \hat{\mathbf{r}}'])^{3/2}}, \quad (14)$$

which renders it extremely useful for our purposes, as we shall see. Eq. (13) are the coefficients in the Legendre series expansion of eq. (14), as shown by, for example, Sansone (1959). Eq. (14) is remarkable in that it allows us to calculate a truly non-bandlimited (and thus spatially less oscillatory) kernel of the form (11) with extreme computational efficiency. For other examples of finite closed-form expressions from infinite expansions with geophysically motivated symbols, see, for example, Whaler & Gubbins (1981), Shure *et al.* (1982) and Parker (1994).

2.3 Harmonic splines

Throughout this paper, let $\mathcal{F} \equiv \{\mathcal{F}_q\}_{q=1, \dots, N}$ be a set of bounded, real-valued, linear, continuous functionals on \mathcal{H} . As an example, identifying $c^{-1}(\hat{\mathbf{r}})$ of eq. (1) as a scalar function $f : \Omega \rightarrow \mathbb{R}$, which associates a phase slowness with every point on the sphere, we may rewrite the linear integral equation (eq. 1) as, simply

$$\mathcal{F}_q(f) := \int_{\gamma_q} f(\hat{\mathbf{r}}) d\gamma = t_q \quad \text{for } q = 1, \dots, N. \quad (15)$$

This again formulates the surface wave tomography problem as: given a set of known traveltimes and the corresponding set $\{\mathcal{F}_q\}_{q=1, \dots, N}$ of linear functionals, find the unknown slowness distribution $f \in \mathcal{H}$ such that (15) holds true. Before proceeding, we note that eq. (15) represents a ‘ray-theoretical’ measurement at infinite frequency; the integral is over the geometric ray path. Accounting for finite-frequency effects and measurement strategies would transform the data functional into a volume integral with the appropriate sensitivity kernel (e.g. Dahlen *et al.* 2000; Zhou *et al.* 2004). The functionals \mathcal{F}_q map a scalar field f onto a set of reals t_q ; in the same vein, we define

$$\mathcal{F}_q(K_{\mathcal{H}}[\hat{\mathbf{r}}]) := \int_{\gamma_q} K_{\mathcal{H}}(\hat{\mathbf{r}}, \hat{\mathbf{r}}') d\gamma' \quad \text{for } \hat{\mathbf{r}} \in \Omega, \quad (16)$$

which projects a kernel in two variables onto a field in one, by integrating over the second one. After an additional integration, the result $\mathcal{F}_k(\mathcal{F}_q(K_{\mathcal{H}}))$ is once again a set of reals, as in eq. (15).

Any function $f \in \mathcal{H}$ of the form

$$f(\hat{\mathbf{r}}) = \sum_{k=1}^N a_k \mathcal{F}_k(K_{\mathcal{H}}[\hat{\mathbf{r}}]) \quad \text{for } \hat{\mathbf{r}} \in \Omega, \quad (17)$$

is called a ‘spherical spline’ in \mathcal{H} , relative to \mathcal{F} . If the system \mathcal{F} is linearly independent, then there exists a unique f , out of the set of all possible splines, that satisfies

$$\mathcal{F}_q(f) = t_q \quad \text{for all } q = 1, \dots, N. \quad (18)$$

Let, now, the system of functionals \mathcal{F} be linearly independent. Then the spline interpolation problem (eq. 18)—in our case the tomography problem (eq. 15) for a unique set of paths γ_q —amounts to

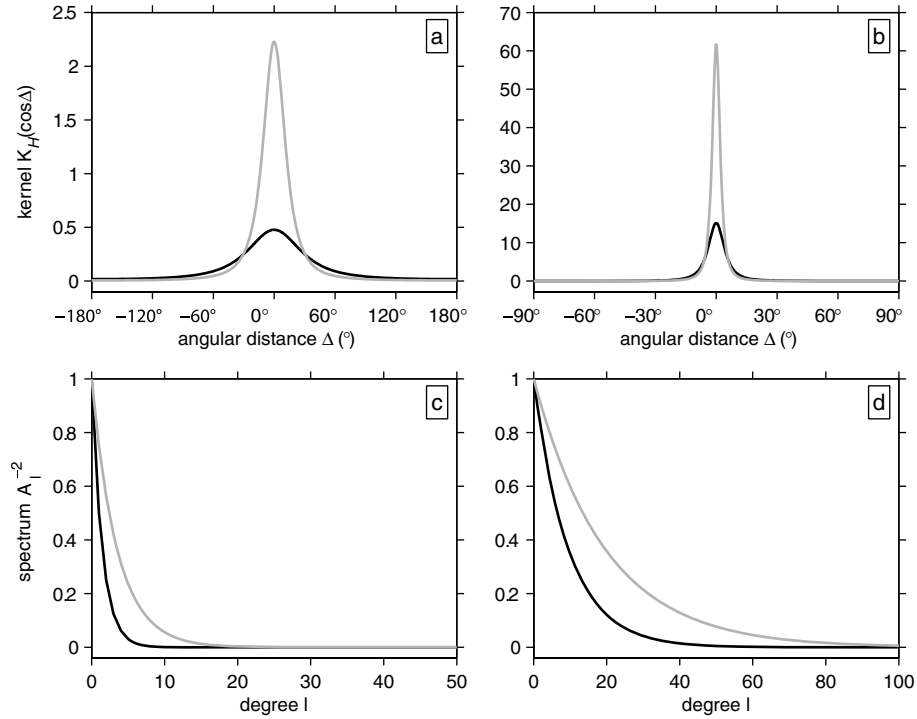


Figure 1. The Abel–Poisson reproducing kernel. (a) and (b) Spatial variation as a function of the angular distance $\Delta = \arccos(\hat{\mathbf{f}} \cdot \hat{\mathbf{f}}')$ between two points $\hat{\mathbf{f}}$ and $\hat{\mathbf{f}}'$ along the surface of the unit sphere, for the parameters $h = 0.50$ (black), $h = 0.75$ (grey) in panel (a), and for $h = 0.90$ (black) and $h = 0.95$ (grey) in panel (b). (c) and (d) Spectrum A_l^{-2} as a function of spherical harmonic degree l , for the same parameter combinations as in panels (a) and (b).

finding the coefficients $\{a_k\}_{k=1, \dots, N}$ from the linear system of equations:

$$\sum_{k=1}^N a_k \mathcal{F}_q(\mathcal{F}_k(K_{\mathcal{H}})) = t_q, \quad (19)$$

as we can see by combining eqs (15) and (17). It also follows that the Gram matrix, whose elements are given by

$$F_{qk} = \mathcal{F}_q(\mathcal{F}_k(K_{\mathcal{H}})), \quad (20)$$

is square and positive definite, and that the spline (eq. 17) satisfying eq. (18) is unique in minimizing the norm $\|f\|_{\mathcal{H}}$. For mathematical details and proofs of the above statements, we refer to Freedon (1999); geophysical insight is imparted by Parker (1994).

To account for imperfect data, the interpolation conditions (eq. 18) can be combined with a smoothing condition, for example, by adding positive constants to the diagonal of the matrix (20) and solving the modified linear equation system

$$\sum_{k=1}^N a_k \mathcal{F}_q(\mathcal{F}_k(K_{\mathcal{H}})) + \rho \sigma_q^2 a_q = t_q \quad (21)$$

for a smoothing level or regularization parameter $\rho > 0$ and a data variance σ_q^2 . In that case, the spline (eq. 17) is ‘approximating’ rather than ‘interpolating’, and may be shown to uniquely minimize the functional

$$\sum_{k=1}^N \left[\frac{\mathcal{F}_k(f) - t_k}{\sigma_k} \right]^2 + \rho \langle f, f \rangle_{\mathcal{H}}, \quad (22)$$

as discussed in detail by Freedon (1999). See also Craven & Wahba (1979) for a related approach on the interval.

An optimal value for ρ can be selected by a variety of methods (Engl *et al.* 1996; Aster *et al.* 2005), such as by ‘generalized cross-validation’ (Craven & Wahba 1979) or from the knick-point

of the so-called ‘*L*-curve’ (Lawson & Hanson 1974; Hansen 1992) of the solution norm $\|f\|_{\mathcal{H}}$ for a particular value of ρ plotted against $\|\sum_k F_{qk} a_k - t_q\|$, the norm of the misfit—see Amirbekyan (2007) for practical examples.

2.4 Mathematical context

It is worth noting that Nashed & Wahba (1974, 1975) used reproducing-kernel based approaches to approximate the generalized inverse of an operator from an arbitrary Hilbert space into a set of real-valued functions on an interval or in-between two such sets. Subsequently, Engl (1982, 1983a) established the idea of using reproducing kernels to regularize ill-posed problems for Fredholm integral equations of the first kind on an interval, at the same time suggesting the probable applicability of this method to other reproducing-kernel Hilbert spaces. Generalizations to arbitrary real Hilbert spaces can be found in Engl (1983b), which in turn inspired the further developments of Amirbekyan (2007) and Amirbekyan & Michel (2008).

Other approaches to construct approximating tools out of reproducing-kernel Hilbert spaces exist (see, e.g. Saitoh *et al.* 2003; Bolotnikov & Rodman 2004; Saitoh 2005). While all of them are related to the harmonic splines used here inasmuch as they use reproducing kernels to regularize ill-posed problems, they are, nevertheless, very different in the details.

Finally, it should be remarked that the harmonic splines of this paper are related to the spherical wavelets of Windheuser (1995) and Freedon & Windheuser (1997), noting that the wavelets are differences of reproducing kernels, which are called ‘scaling functions’ in this context (Freedon *et al.* 1998).

3 APPLICATION TO TOMOGRAPHY

We return to the specific problem of determining an earth model, that is, the geographical variations of the inverse phase speed $c^{-1}(\hat{\mathbf{r}})$ —or slowness—of seismic surface waves from a set of great-circle integrals—otherwise known as traveltimes measurements. These path integrals are the linear continuous functionals \mathcal{F} of Section 2.3. They owe their linearity to the linearity of integration, and using the boundedness of the phase slowness and the ray paths, it can easily be shown that these functionals are continuous as well (Amirbekyan 2007). Furthermore, we assume that every path is measured exactly once; as a consequence, the $\mathcal{F}_q(c^{-1})$, $q = 1, \dots, N$ are linearly independent (Amirbekyan 2007), and an earth model can be constructed by solving the interpolation problem (eq. 19) or the approximation problem (eq. 21), depending on the accuracy of the measurements.

Interpolating, or approximating, the unknown phase slowness by a harmonic spline requires evaluating eqs (17) and (19) and inverting the square matrix (20). Such calculations are greatly aided by, and explain the motivation behind, a parametrization approach rooted in spherical harmonics. In this section, we give constructive proofs for two different methodologies to implement a harmonic-spline based parametrization of a surface wave earth model.

3.1 First method

The stationary ray path taken by the surface wave across the surface of the Earth, γ , is a great circle, the geodesic minimal arc between the source and the receiver. The entries of the Gram matrix (20) which we require, are thus integrals of the form

$$\int_{\gamma_q} \left[\int_{\gamma_k} K_{\mathcal{H}}(\hat{\mathbf{r}}, \hat{\mathbf{r}}') d\gamma' \right] d\gamma = \sum_{l=0}^{\infty} \sum_{m=-l}^l A_l^{-2} \int_{\gamma_q} Y_{lm}(\hat{\mathbf{r}}) d\gamma \int_{\gamma_k} Y_{lm}(\hat{\mathbf{r}}') d\gamma', \quad (23)$$

as seen by substituting the expressions (10) and (15) into eq. (20).

Equations such as eq. (23), which are in terms of the real spherical harmonics Y_{lm} of eq. (4), are of a form that lends itself easily to numerical implementation without integration, since the complex spherical harmonics \mathcal{Y}_{lm} , defined in eqs (5)–(7), satisfy the explicit expression (Dahlen & Tromp 1998, p. 930)

$$\int_{\gamma} \mathcal{Y}_{lm}(\hat{\mathbf{r}}) d\gamma = \sum_{m'=-l}^l (i/m') X_{lm'}(\pi/2) (1 - e^{im'\Delta}) \times \mathcal{D}_{m'm}^{(l)}(\alpha, \beta, \delta), \quad (24)$$

where X_{lm} is the normalized Legendre polynomial defined in eq. (6), Δ is the source–receiver epicentral angular distance, $\mathcal{D}_{m'm}^{(l)}$ is a Wigner rotation matrix whose elements can be computed efficiently by recursion (Edmonds 1996; Blanco *et al.* 1997; Dahlen & Tromp 1998; Masters & Richards–Dinger 1998) and, finally, α , β and δ are Euler angles that depend on Δ and the geographical coordinates of the source (θ_S, ϕ_S) and the receiver (θ_R, ϕ_R) as follows:

$$\tan \alpha = \frac{\sin \theta_R \cos \theta_S \cos \phi_R - \cos \theta_R \sin \theta_S \cos \phi_S}{\cos \theta_R \sin \theta_S \sin \phi_S - \sin \theta_R \cos \theta_S \sin \phi_R}, \quad (25)$$

$$\cos \beta = \frac{\sin \theta_R \sin \theta_S \sin(\phi_R - \phi_S)}{\sin \Delta}, \quad (26)$$

$$\tan \delta = \frac{\cos \theta_S \cos \Delta - \cos \theta_R}{\cos \theta_S \sin \Delta}. \quad (27)$$

After obtaining the model coefficients a_k , $k = 1, \dots, N$ by solving eqs (19) or (21), an earth model in the function space \mathcal{H} is obtained via eq. (17):

$$f(\hat{\mathbf{r}}) = \sum_{k=1}^N a_k \sum_{l=0}^{\infty} \sum_{m=-l}^l A_l^{-2} \left[\int_{\gamma_k} Y_{lm}(\hat{\mathbf{r}}') d\gamma' \right] Y_{lm}(\hat{\mathbf{r}}), \quad (28)$$

which presents no additional numerical burden.

3.2 Second method

The computation scheme outlined above has an alternative. Rather than using the analytical great-circle integrals (eq. 24), we may use a parametrized version of the great-circle equations and perform the resulting integrals numerically. This works for any arbitrary function; in the context of spherical splines, we write the entries of the Gram matrix (20) using eqs (11) and (15) as

$$\int_{\gamma_q} \left[\int_{\gamma_k} K_{\mathcal{H}}(\hat{\mathbf{r}}, \hat{\mathbf{r}}') d\gamma' \right] d\gamma = \sum_{l=0}^{\infty} A_l^{-2} \left(\frac{2l+1}{4\pi} \right) \int_{\gamma_q} \int_{\gamma_k} P_l(\hat{\mathbf{r}} \cdot \hat{\mathbf{r}}') d\gamma' d\gamma. \quad (29)$$

Taking $\hat{\mathbf{r}}_S$ and $\hat{\mathbf{r}}_R$ to be the source and receiver points on the unit sphere, we let $\mathbf{w} = \hat{\mathbf{r}}_R - (\hat{\mathbf{r}}_S \cdot \hat{\mathbf{r}}_R) \hat{\mathbf{r}}_S$ and $\hat{\mathbf{w}} = \mathbf{w} / \|\mathbf{w}\|$, for which $\hat{\mathbf{r}} \cdot \hat{\mathbf{w}} = 0$. Then, the parametric equation of the great circle between $\hat{\mathbf{r}}_S$ and $\hat{\mathbf{r}}_R$ can be written as

$$\hat{\mathbf{r}}_{\gamma}(\tau) = \hat{\mathbf{r}}_S \cos \tau + \hat{\mathbf{w}} \sin \tau \quad \text{with} \quad 0 \leq \tau \leq \Delta, \quad (30)$$

where the epicentral distance $\Delta = \arccos(\hat{\mathbf{r}}_S \cdot \hat{\mathbf{r}}_R)$ and, as expected, $\hat{\mathbf{r}}_{\gamma}(0) = \hat{\mathbf{r}}_S$ and $\hat{\mathbf{r}}_{\gamma}(\Delta) = \hat{\mathbf{r}}_R$. With the great circle γ thus parametrized by the coordinate function $\hat{\mathbf{r}}_{\gamma}(\tau)$ and noting that $\|\hat{\mathbf{r}}_{\gamma}(\tau)\| = 1$ everywhere on the interval, the line integrals

$$\int_{\gamma_q} \int_{\gamma_k} P_l(\hat{\mathbf{r}} \cdot \hat{\mathbf{r}}') d\gamma' d\gamma = \int_0^{\Delta_q} \int_0^{\Delta_k} P_l(\hat{\mathbf{r}}_{\gamma_q}(\tau) \cdot \hat{\mathbf{r}}_{\gamma_k}(\tau')) d\tau' d\tau \quad (31)$$

can be evaluated using standard numerical quadrature methods. Once the model coefficients a_k , $k = 1, \dots, N$ have been determined from eqs (19) or (21), the earth model is calculated from eq. (17) as

$$f(\hat{\mathbf{r}}) = \sum_{k=1}^N a_k \sum_{l=0}^{\infty} A_l^{-2} \left(\frac{2l+1}{4\pi} \right) \int_0^{\Delta_k} P_l(\hat{\mathbf{r}}_{\gamma_k}(\tau) \cdot \hat{\mathbf{r}}) d\tau. \quad (32)$$

3.3 Second method: a special case

A ‘third’ method applies the second method to the special but important case where the reproducing kernel is of the Abel–Poisson type of eq. (14), which was previously shown in Fig. 1. The Gram matrix becomes the numerically doable

$$\int_{\gamma_q} \left[\int_{\gamma_k} K_{\mathcal{H}}(\hat{\mathbf{r}}, \hat{\mathbf{r}}') d\gamma' \right] d\gamma = \left(\frac{1-h^2}{4\pi} \right) \times \int_0^{\Delta_q} \int_0^{\Delta_k} \{1 + h^2 - 2h[\hat{\mathbf{r}}_{\gamma_q}(\tau) \cdot \hat{\mathbf{r}}_{\gamma_k}(\tau')]\}^{-3/2} d\tau' d\tau, \quad (33)$$

and the earth model, once the coefficients a_k have been recovered through eqs (19) or (21), is obtained from

$$f(\hat{\mathbf{r}}) = \sum_{k=1}^N a_k \left(\frac{1-h^2}{4\pi} \right) \times \int_0^{\Delta_k} \{1+h^2-2h[\hat{\mathbf{r}}_{\gamma_k}(\tau) \cdot \hat{\mathbf{r}}]\}^{-3/2} d\tau. \quad (34)$$

4 NUMERICAL TESTS

Here, we present the results of numerical tests conducted to verify and illustrate the performance of the parametrization of surface wave models by harmonic splines. Inversion tests come in many flavours (see, e.g. Spakman & Nolet 1988). Nevertheless, the collective of results that we will show, in our opinion, convincingly argues for the utility, versatility, and reliability of our new method.

Before we discuss the details, we note that all tests depend on being able to produce a ‘synthetic’ data set, that is, we have to be able to specify an arbitrary earth model $f(\hat{\mathbf{r}}_l)$ at a set of points $\hat{\mathbf{r}}_l$ on the sphere and produce a set of theoretical traveltimes for it. We can do this as follows for a model that is in the form

$$f(\hat{\mathbf{r}}) = \sum_{k=1}^N a_k K_{\gamma_k}(\hat{\mathbf{r}}_k, \hat{\mathbf{r}}), \quad (35)$$

where the $\{\hat{\mathbf{r}}_k\}_{k=1,\dots,N}$ are pairwise distinct points on the unit sphere. We obtain the required coefficients $\{a_k\}_{k=1,\dots,N}$ by solving the linear equation system

$$\sum_{k=1}^N a_k K_{\gamma_l}(\hat{\mathbf{r}}_k, \hat{\mathbf{r}}_l) = f(\hat{\mathbf{r}}_l) \quad \text{for all } l = 1, \dots, N. \quad (36)$$

The matrix with elements $K_{\gamma_l}(\hat{\mathbf{r}}_k, \hat{\mathbf{r}}_l)$ is regular since every system of pairwise distinct points $(\hat{\mathbf{r}}_k, \hat{\mathbf{r}}_l)$ is a ‘fundamental system’ (Schreiner 1997b). The traveltimes synthetics for great-circle paths γ_q are then calculated according to eq. (15), and thus, given by

$$t_q = \sum_{k=1}^N a_k \int_{\gamma_q} K_{\gamma_k}(\hat{\mathbf{r}}_k, \hat{\mathbf{r}}) d\gamma, \quad (37)$$

computed via the numerical methods discussed in Section 3.

All forthcoming tests use the Abel–Poisson kernel (eqs 13–14) with $h = e^{-0.2}$ or $h = e^{-0.05}$, as indicated in the captions. As shown by Fig. 1, the parameter, or symbol, $h \in (0, 1)$ determines the hat-width of the kernel K_{γ} : the closer h is to 1, the narrower is the kernel width. Currently, there is no general method to determine an optimal symbol for each particular problem; the optimal choice of h depends on the physics of the problem (e.g. Zhou *et al.* 2004), the spatial density of the given data and the *a priori* information about the smoothness of the underlying model (e.g. Montagner 1986). The integral terms representing the matrix components and the spline basis were calculated approximately with the composite trapezoidal rule, as in Section 3.3. All inversions were performed using Cholesky factorization.

We consider three sets of great-circle paths for simulating data and evaluating model recovery (Fig. 2). The first is a global collection of 2469 earthquakes and 199 stations (Fig. 2a) yielding 8490 surface wave paths (Fig. 2b); a situation based on, if not identical to, the ray path coverage in the models of Rayleigh-wave phase speeds at 80s period, obtained by Trampert & Woodhouse (1995, 1996, 2001). The second is an admittedly unrealistic, but challenging, regional case with 500 unique ray paths covering the Australian continent (Figs 2c and d). Both sets are the basis for the tests discussed in Section 4.1 and 4.2. The third is a combination experiment; its path coverage and inversion results appear in a separate figure and are discussed in Section 4.3.

4.1 Checkerboard tests

As a first experiment we performed a series of classical checkerboard tests. We generated a synthetic model by the equation

$$f(\theta, \phi) = 4 + 0.2 \sin(a\theta) \sin(b\phi), \quad (38)$$

in colatitude θ and longitude ϕ , with $a = 8$, $b = 10$ for Fig. 3 and $a = 16$, $b = 20$ for Figs 4 and 6. This amounts to a phase-speed model whose mean is 4 km s^{-1} and whose deviations therefrom do not exceed ± 5 per cent. We calculated theoretical traveltimes by direct numerical integration and added 1 per cent data noise to them in the cases indicated in the figure legends.

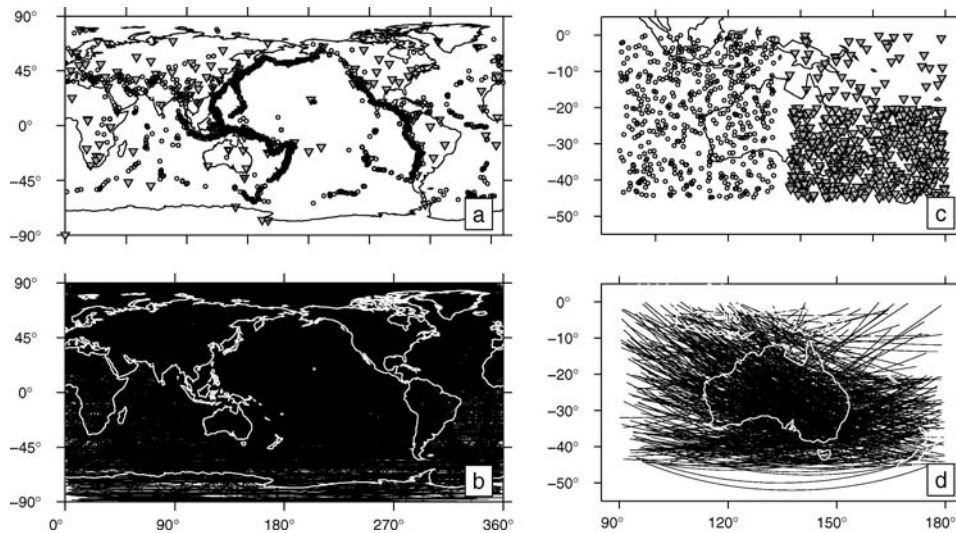


Figure 2. Data coverage for the numerical tests. Sources (white filled circles), receivers (grey filled triangles) and great-circle paths (black curves) for synthetic global (a and b) and regional (c and d) modelling. The global experiment has 8490 ray paths and is inspired by the data sets compiled by Trampert & Woodhouse (1995, 1996, 2001). The regional experiment is a synthetic in the truest sense of the word and counts 500 unique ray paths.

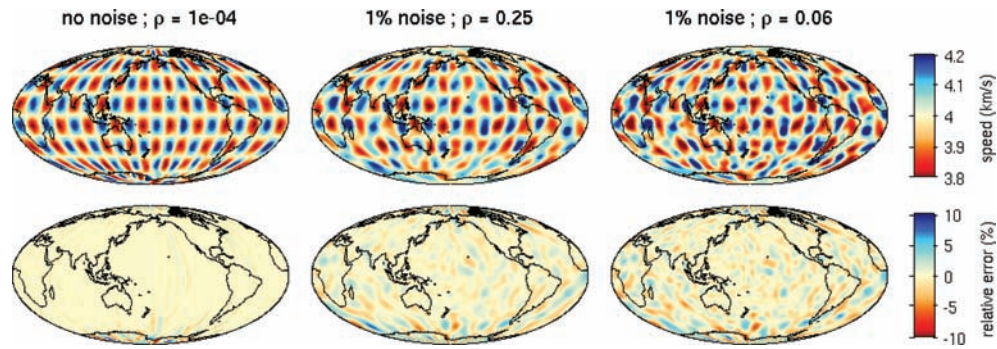


Figure 3. Results from synthetic ‘checkerboard’ inversion tests using the global path coverage shown in Fig. 2(b) and the Abel–Poisson kernel with $h = e^{-0.2}$. Top row: recovery (in km s^{-1}), by eqs (21) and (22), of the input pattern, for varying noise levels and regularization parameters ρ as shown in the legend. Bottom row: reconstruction error, in per cent relative to 4 km s^{-1} , the mean of the model input.

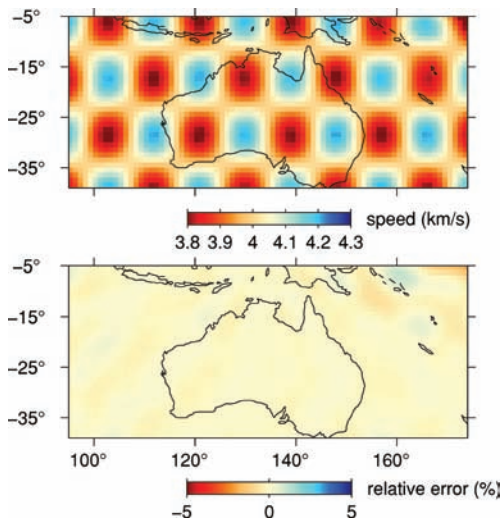


Figure 4. Results from synthetic ‘checkerboard’ inversion tests using the regional path coverage shown in Fig. 2(d) and the Abel–Poisson kernel with $h = e^{-0.2}$. Top: recovered pattern, in km s^{-1} . Bottom: recovery error relative to 4 km s^{-1} , in per cent.

Fig. 3 reports on the results for the global ray coverage of Fig. 2(b). The inversion was regularized as in eqs (21) and (22) with regularization parameters $\rho = 10^{-4}$, 0.25 and 0.06, respectively, as shown in the legend. In all cases shown, the histograms of the residuals relative to 4 km s^{-1} are reasonably normally distributed with means of 0.06, 0.11 and 0.06 per cent, standard deviations of 1.47, 1.80 and 2.01 per cent and root-mean-squared recovery errors (rmse) of 0.059, 0.072 and 0.080 km s^{-1} , respectively, corresponding to the three noise and regularization levels shown in Fig. 3. A result using the contrived regional path coverage of Fig. 2(d), without noise and using $\rho = 10^{-5}$, is shown in Fig. 4. Here, too, the recovery is excellent, with a mean error of -0.001 per cent, a standard deviation of 0.09 per cent and an rmse of 0.002 km s^{-1} over the Australian model domain shown.

We repeated all experiments using the ‘standard’ spherical harmonic (up to a bandwidth of degree 39) inversion method, described in detail by Trampert & Woodhouse (1995). For regularization and to reduce ringing (Trampert & Woodhouse 1995; Trampert & Snieder 1996; Trampert & Woodhouse 2003), they advocate using an *a priori* diagonal covariance matrix on the spherical harmonic expansion coefficients whose elements are given by

$$\lambda^{-1}[l(l+1)]^{-2}, \quad (39)$$

where l is the degree of the corresponding spherical harmonic and λ is a smoothing parameter. Much like the regularization parameter ρ in the harmonic-spline method, determining the smoothing parameter λ for the spherical harmonic method is somewhat of an art that can, however, be made more quantitative by considering the L -curve showing the trade-off of solution norm versus the model misfit, or by ‘generalized cross-validation’ (see Section 2.3). In this suite of synthetic experiments with known input, however, we simply selected the value of λ that yielded the lowest rmse. The chosen $\lambda = 10^{-7}$, 10^{-5} and 10^{-6} and the corresponding rmse were 0.058, 0.070 and 0.093 km s^{-1} ; in other words, statistically indistinguishable from the harmonic-spline results for the global case reported above. For the Australian experiment, the best value was $\lambda = 10^{-9}$ and the resulting statistics 7×10^{-5} per cent, 0.31 per cent and 0.006 km s^{-1} for the mean, standard deviation and rms error, respectively.

We realize that not every possible situation of data and model configuration can be tested with these few simple experiments, nevertheless, conclude that these checkerboard experiments do illustrate that the harmonic-spline method reveals itself to be a practical and reliable method to tackle large-scale surface wave tomographic experiments on global as well as regional scales.

4.2 Hidden-object tests

Checkerboard tests are not uncontroversial (see, e.g. L ev eque *et al.* 1993)—not in the least, because the ‘correct’ answer is a known, and most certainly un-Earth-like, phase-speed distribution. For this reason, we conducted another suite of experiments with an input model that itself is the result of a test inversion of Rayleigh-wave phase-speed measurements from the Trampert & Woodhouse (1995, 1996, 2001) data set—to which we added a patch of an anomalously low velocity (3 km s^{-1}) as a ‘hidden object’, clearly visible in Fig. 5.

The inversion results, using the Abel–Poisson harmonic-spline method and the global path coverage of Fig. 2(b), are shown in Fig. 5. The recovery is very good—the statistics for this example are 0.14 per cent mean, 1.10 per cent standard deviation of the relative and 0.045 km s^{-1} rms error. For comparison, the inversion using standard spherical harmonic inversions with a regularization parameter of $\lambda = 10^{-5}$ yields values of 0.02 per cent, 1.18 per cent and 0.048 km s^{-1} in these categories, respectively, though it is noticeable that the error in the harmonic-spline reconstruction is more concentrated around the area of the anomalous object than in the recovery, parametrized by global spherical harmonic basis functions (Amirbekyan 2007), as expected.

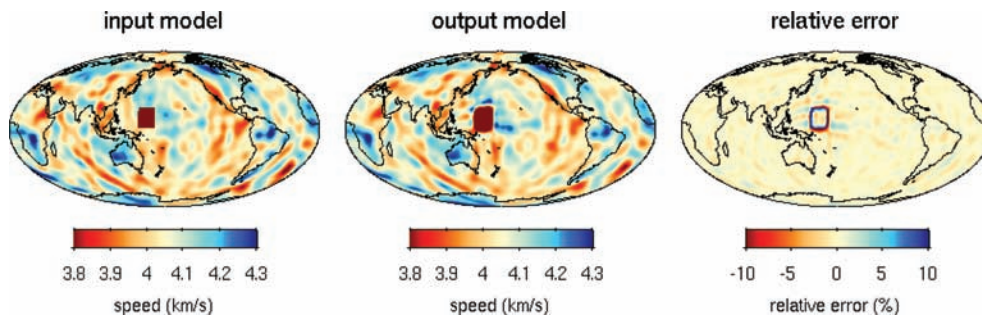


Figure 5. Inversion test with a realistic, Earth-like phase-speed distribution plus a low-velocity ‘hidden object’, recovered by the harmonic-spline method with the global path coverage shown in Fig. 2(b), the Abel–Poisson kernel with $h = e^{-0.2}$ and a regularization parameter $\rho = 0.05$. Relative error is with respect to the average of the input model of 4.06 km s^{-1} .

We repeated the above tests after adding random noise to the data sets and comparing the absolute and relative performance of the harmonic-spline and spherical harmonic methods. The sensitivity of the spline method to measurement errors is not larger than that of the spherical harmonic method (Amirbekyan 2007).

4.3 Mixed-resolution tomography

In the two previous sections, we assessed the performance of the new harmonic-spline method in recovering global or regional wave speed anomalies. We argued that the harmonic splines are competitive with smoothed spherical-harmonic parametrization based on simple metrics such as the rmse. Upon casual inspection, the improvements, however, were slight, and the skeptical seismologist might well wonder whether the payoff of investing in a new methodology, however mathematically elegant, is sufficient. In this paragraph, we hope to allay any fears that it might not be.

Seismologists are increasingly faced with constructing wave speed models that combine global and regional data sets into a single inversion. A recent example is the ongoing deployment of the USARRAY (<http://www.iris.edu/USArray>), which is in the process of densifying the North American station coverage multiple times with respect to the existing global networks (Romanowicz & Giardini 2001; Romanowicz 2008). For such problems, parametrizations ideally are adaptive and locally adjusted to the model resolution. In the literature, such approaches come in a variety of flavours, using block subdivisions, (e.g. Abers & Roecker 1991; Bijwaard *et al.* 1998; Káráson & van der Hilst 2000; Simons *et al.* 2002), irregularly distributed nodes (e.g. Debayle & Sambridge 2004; Nolet & Montelli 2005) or cubic B-splines on dyadically subdivided spherical tessellations (e.g. Wang *et al.* 1998; Boschi *et al.* 2004; Nettles & Dziewoński 2008). All these require an initial step of ‘grid design’, based on some measure of expected resolution. None of them are proper mathematically speaking ‘multi-resolution’ (*sensu* Mallat 1989)—global seismological parametrizations by spherical wavelets being still in their infancy (e.g. Chiao & Kuo 2001; Chevrot & Zhao 2007; Loris *et al.* 2007).

The approach taken with the harmonic spherical splines in this paper is tested with respect to the particular complications introduced by mixing global and regional ray coverage. Our free parameters are the type of splines used, that is, the symbol A_l , which, as shown in eqs (10) and (11), determines the properties of the reproducing kernel $K_{\mathcal{H}}$ and thus of the function space of the solution, and the regularization parameter ρ of eq. (21) determining the trade-off between data fit and model norm. The Gram matrix (20) is always square with the dimensions of the number of ray paths $N \times N$. For

the tests, we remain faithful to the Abel–Poisson kernel (13), but we vary the values of $0 < h < 1$ and ρ .

For comparison, we show the results of ‘industry-standard’ smoothed spherical harmonic inversions (e.g. Boschi *et al.* 2004), where decisions are to be made on the truncation bandwidth L , which determines the number of model parameters as $(L + 1)^2$ and the size of the normal matrix $N \times (L + 1)^2$, and the regularization parameter λ in eq. (39). For the tests we varied both L and λ .

The input model is the checkerboard pattern generated by eq. (38) with $a = 16$ and $b = 20$, which has power dominantly between spherical harmonic degrees 25–35. Some results are shown in Fig. 6, with performance metrics listed in Table 1. As expected, smoothed spherical harmonic inversions perform increasingly better as the truncation degree increases, but all of them continue to suffer severely from wild swings in the areas without any data coverage. For the optimal (as per the rmse) parameter settings in the harmonic-spline inversion (Abel–Poisson with $h = e^{-0.05}$ and $\rho = 1 \times 10^{-3}$), the recovery is also very good in the areas of dense path coverage (North America and Australia) but only a small amount of structure is introduced in the areas largely devoid of ray paths. The spline-based rmse in the regions marked by the black boxes in Fig. 6(h) is very low. More importantly, it is quite significantly lower than the equivalent rmse in those areas under the spherical harmonic parametrization. The localizing character of the harmonic splines has clear advantages over the traditional spectral approach: we conclude that the new method holds its own in a variety of challenging settings.

Elsewhere, Amirbekyan (2007) shows best-fit inversion results and tests based upon them, using actual Rayleigh and Love wave phase-speed anomaly data, measured on individual seismograms compiled by Trampert & Woodhouse (1995, 1996, 2001). Here, we refrain from presenting the results in these pages until they can be presented with the proper seismological validation and geological interpretation that they require but that, unfortunately, falls outside of the scope of this methodological presentation.

5 CONCLUSIONS

The inverse problem of interpolation or approximation using harmonic-spline basis functions is a good alternative to current methods in seismic surface wave tomography, which are based on purely local (blocks) or purely global (spherical harmonics) basis functions. Harmonic spherical splines pair the analytical advantages of the spherical harmonics, most notably their efficient integration over great-circle paths, with a localizing character that lends itself equally well to the parametrization of global as well as regional (or mixed-resolution) phase speed models made from traveltimes

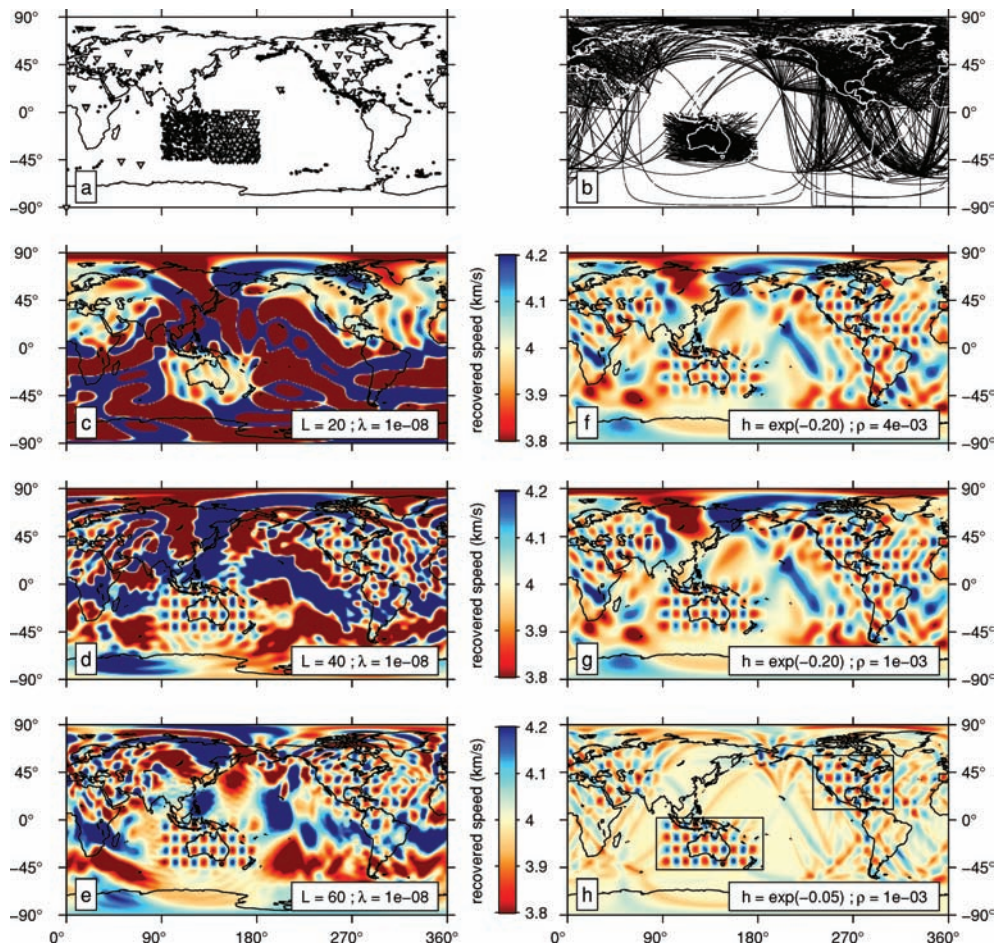


Figure 6. Inversion tests for a global checkerboard input pattern with stations as in panel (a), a highly heterogeneous path coverage shown in (b) and recovered (c–e) via the spherical harmonic method at varying bandwidths L and regularization parameters λ and (f–h) by harmonic splines with the $h = e^{-0.05}$ Abel–Poisson kernel and various regularization parameters ρ , as shown in the legend. See Table 1 for a statistical description of the global results and of those for the North American and Australian subregions (black boxes).

Table 1. Recovery of a checkerboard pattern (see Section 4.3 and Fig. 6) using spherical harmonics (bandwidth L and regularization parameter λ) or splines (with Abel–Poisson kernel of symbol h and regularization parameter ρ). Shown are the root-mean-squared recovery errors (rmse) for the tests depicted in Fig. 6. The rmse are reported for the global modelling domain as well as for the well-covered North American and Australian regions outlined by black boxes in Fig. 6(h).

L	λ	rmse (global)	rmse (N. Am.)	rmse (Aust.)
20	10^{-8}	$6.79 \times 10^{+2}$	2.35×10^{-1}	4.52×10^{-1}
40	10^{-8}	4.63×10^{-1}	1.40×10^{-1}	8.15×10^{-2}
60	10^{-8}	1.84×10^{-1}	7.09×10^{-2}	5.63×10^{-2}
h	ρ	rmse (global)	rmse (N. Am.)	rmse (Aust.)
$e^{-0.20}$	0.004	1.21×10^{-1}	6.07×10^{-2}	7.13×10^{-2}
$e^{-0.20}$	0.001	1.30×10^{-1}	6.01×10^{-2}	6.45×10^{-2}
$e^{-0.05}$	0.001	8.98×10^{-2}	4.87×10^{-2}	5.30×10^{-2}

measurements. The method is based on spatially localizing reproducing-kernel basis functions that effectively reduce the vast model space to contain only models of a certain well-defined smoothness. In the case of the Abel–Poisson kernel, this smoothness is characterized by a single parameter, the symbol of the kernel that determines the decay of its spectral power, and thus, the spatially

localizing behaviour. Great-circle integrations based on the Abel–Poisson kernel expansion can be performed semi-analytically with great accuracy. The tomographic inversion problem then amounts to the inversion of a square and positive-definite Gram matrix, to which an additional regularization matrix can be added, with a trade-off parameter whose ideal value can be determined to depend on the estimated data noise and a user-acceptable compromise between model smoothness and data misfit. This type of splines is not confined to the unit sphere, the case dealt with in this paper—volumetric reproducing-kernel based approaches suitable for fully 3-D inversions, including of body-wave data, are on the horizon (Amirbekyan & Michel 2008).

ACKNOWLEDGMENTS

The authors express their gratitude to the ‘DFG-Graduiertenkolleg Mathematik und Praxis’ of the Department of Mathematics at the University of Kaiserslautern, which financed the visits of FJS and Jeannot Trampert to Kaiserslautern. AA and VM wish to thank Jeannot Trampert from Utrecht University for very valuable discussions and for providing the data sets which were used in the numerical tests. AA acknowledges financial support from German Academic Exchange Service (DAAD), the Forschungsschwerpunkt ‘Mathematik und Praxis’, University of Kaiserslautern and the

International School for Graduate Studies (ISGS), University of Kaiserslautern. VM acknowledges financial support from the German Research Foundation (DFG), project MI 655/2-1. FJS acknowledges financial support from a NERC Young Investigators' Award (NE/D521449/1), a Nuffield Foundation grant for Newly Appointed Lecturers (NAL/01087/G) and NSF grants EAR-0710860 and EAR-0105387. We thank the Associate Editor, Jeannot Trampert, Malcolm Sambridge and an anonymous reviewer for insightful comments that helped clarify and improve the paper. Computer code is made available on www.frederik.net.

REFERENCES

- Abers, G.A. & Roecker, S.W., 1991. Deep structure of an arc-continent collision: earthquake relocation and inversion for upper mantle P and S wave velocities beneath Papua New Guinea, *J. geophys. Res.*, **96**(B4), 6379–6401.
- Aki, K., Christofferson, A. & Husebye, E.S., 1977. Determination of the three-dimensional seismic structure of the lithosphere, *J. geophys. Res.*, **82**(2), 277–296.
- Amirbekyan, A., 2007. The application of reproducing kernel based spline approximation to seismic surface and body wave tomography: theoretical aspects and numerical results, *PhD thesis*, Geomathematics Group, Department of Mathematics, University of Kaiserslautern, available at: <http://kluedo.uni-kl.de/volltexte/2007/2103/>.
- Amirbekyan, A. & Michel, V., 2008. Splines on the 3-dimensional ball and their application to seismic body wave tomography, *Inverse Problems*, **24**, 015022, doi:10.1088/0266-5611/24/1/015022.
- Aronszajn, N., 1950. Theory of reproducing kernels, *Trans. Am. Math. Soc.*, **68**(3), 337–404.
- Aster, R.C., Borchers, B. & Thurber, C.H., 2005. *Parameter Estimation and Inverse Problems*, Vol. 90: International Geophysics Series, Elsevier Academic Press, San Diego, CA.
- Backus, G.E., 1970a. Inference from inadequate and inaccurate data, I, *Proc. Natl. Acad. Sc.*, **65**(1), 1–7.
- Backus, G.E., 1970b. Inference from inadequate and inaccurate data, II, *Proc. Natl. Acad. Sc.*, **65**(2), 281–287.
- Backus, G.E., 1970c. Inference from inadequate and inaccurate data, III, *Proc. Natl. Acad. Sc.*, **67**(1), 282–289.
- Backus, G.E. & Gilbert, F., 1968. The resolving power of gross Earth data, *Geophys. J. R. astr. Soc.*, **16**(2), 169–205.
- Backus, G.E. & Gilbert, F., 1970. Uniqueness in the inversion of inaccurate gross Earth data, *Phil. Trans. R. Soc. Lond., A*, **266**, 123–192.
- Backus, G.E., Parker, R.L. & Constable, C.G., 1996. *Foundations of Geomagnetism*, Cambridge University Press, Cambridge, UK.
- Bijwaard, H., Spakman, W. & Engdahl, E.R., 1998. Closing the gap between regional and global travel time tomography, *Geophys. J. Int.*, **103**(B12), 30055–30078.
- Blanco, M.A., Flórez, M. & Bermejo, M., 1997. Evaluation of the rotation matrices in the basis of real spherical harmonics, *J. Mol. Struct. (Theochem)*, **419**, 19–27.
- Bolotnikov, V. & Rodman, L., 2004. Remarks on interpolation in reproducing kernel Hilbert spaces, *Houston J. Math.*, **30**(2), 559–576.
- Boschi, L. & Dziewoński, A.M., 1999. High- and low-resolution images of the Earth's mantle. Implications of different approaches to tomographic modeling, *J. geophys. Res.*, **104**(B11), 25 567–25 594.
- Boschi, L., Ekström, G. & Kustowski, B., 2004. Multiple resolution surface wave tomography: the Mediterranean basin, *Geophys. J. Int.*, **157**, 293–304, doi:10.1111/j.1365-246X.2004.02194.x.
- Byerly, W.E., 1893. *An Elementary Treatise on Fourier's Series and Spherical, Cylindrical, and Ellipsoidal Harmonics*, Ginn & Co., Boston, MA.
- Chevrot, S. & Zhao, L., 2007. Multiscale finite-frequency Rayleigh wave tomography of the Kaapvaal craton, *Geophys. J. Int.*, **169**(1), 201–215, doi:10.1111/j.1365-246X.2006.03289.x.
- Chiao, L.-Y. & Kuo, B.-Y., 2001. Multiscale seismic tomography, *Geophys. J. Int.*, **145**, 517–527, doi:10.1046/j.0956-540x.2001.01403.x.
- Craven, P. & Wahba, G., 1979. Smoothing noisy data with spline functions: estimating the correct degree of smoothing by the method of generalized cross-validation, *Numer. Math.*, **31**, 377–403.
- Dahlen, F.A. & Tromp, J., 1998. *Theoretical Global Seismology*, Princeton University Press, Princeton, NJ.
- Dahlen, F.A., Hung, S.-H. & Nolet, G., 2000. Fréchet kernels for finite-frequency traveltimes—I. Theory, *Geophys. J. Int.*, **141**(1), 157–174.
- Debayle, E. & Sambridge, M., 2004. Inversion of massive surface wave data sets: model construction and resolution assessment, *J. geophys. Res.*, **109**, B02316, doi:10.1029/2003JB002652.
- Doornbos, D.J., ed., 1988. *Seismological Algorithms: Computational Methods and Computer Programs*, Academic Press, San Diego, CA.
- Dziewoński, A.M., 1984. Mapping the lower mantle: determination of lateral heterogeneity in P velocity up to degree and order 6, *J. geophys. Res.*, **89**(B7), 5929–5952.
- Dziewoński, A.M. & Anderson, D.L., 1981. Preliminary Reference Earth Model, *Phys. Earth planet. Inter.*, **25**, 297–356.
- Edmonds, A.R., 1996. *Angular Momentum in Quantum Mechanics*, Princeton University Press, Princeton, NJ.
- Ekström, G., Tromp, J. & Larson, E.W.F., 1997. Measurements and global models of surface wave propagation, *J. geophys. Res.*, **102**(B4), 8137–8157.
- Engl, H.W., 1982. On least-squares collocation for solving linear integral equations of the first kind with noisy right-hand side, *Boll. Geod. Sc. Aff.*, **41**(3), 291–313.
- Engl, H.W., 1983a. On the convergence of regularization methods for ill-posed linear operator equations, in *Improperly Posed Problems and Their Numerical Treatment*, Vol. 63: International Series of Numerical Mathematics, pp. 81–95, eds Hämmerlin, G. & Hoffmann, K.H., Birkhäuser, Boston.
- Engl, H.W., 1983b. Regularization by least-squares collocation, in *Numerical Treatment of Inverse Problems in Differential and Integral Equations*, pp. 345–354, eds Deuffhard, P. & Hairer, E., Birkhäuser, Boston.
- Engl, H.W., Hanke, M. & Neubauer, A., 1996. *Regularization of Inverse Problems*, Kluwer, Dordrecht.
- Fengler, M.J., Freedon, W. & Michel, V., 2004. The Kaiserslautern multiscale geopotential model SWITCH-03 from orbit perturbations of the satellite CHAMP and its comparison to the models EGM96, UCPH2002.02.0.5, EIGEN-1s and EIGEN-2, *Geophys. J. Int.*, **157**, 499–514.
- Fengler, M.J., Michel, D. & Michel, V., 2006. Harmonic spline-wavelets on the 3-dimensional ball and their application to the reconstruction of the Earth's density distribution from gravitational data at arbitrarily shaped satellite orbits, *Z. Angew. Math. Mech.*, **86**(11), 856–873, doi:10.1002/zamm.200510277.
- Forte, A.M., Dziewoński, A.M. & O'Connell, R.J., 1995. Continent-ocean chemical heterogeneity in the mantle based on seismic tomography, *Science*, **268**(5209), 386–388.
- Freedon, W., 1981a. On spherical spline interpolation and approximation, *Math. Meth. Appl. Sc.*, **3**(44), 551–575.
- Freedon, W., 1981b. On approximation by harmonic splines, *Manuscr. Geod.*, **6**, 193–244.
- Freedon, W., 1999. *Multiscale Modelling of Spaceborne Geodata*, Teubner Verlag, Stuttgart.
- Freedon, W. & Michel, V., 1999. Constructive approximation and numerical methods in geodetic research today—an attempt at a categorization based on an uncertainty principle, *J. Geodesy*, **73**(9), 452–465.
- Freedon, W. & Michel, V., 2004. *Multiscale Potential Theory*, Birkhäuser, Boston, MA.
- Freedon, W. & Schreiner, M., 1995. Non-orthogonal expansions on the sphere, *Math. Meth. Appl. Sc.*, **18**, 83–120.
- Freedon, W. & Windheuser, U., 1997. Combined spherical harmonic and wavelet expansion—a future concept in Earth's gravitational determination, *Appl. Comput. Harmon. Anal.*, **4**, 1–37.

- Freeden, W., Gervens, T. & Schreiner, M., 1998. *Constructive Approximation on the Sphere*, Clarendon Press, Oxford, UK.
- Hager, B.H., Clayton, R.W., Richards, M.A., Comer, R.P. & Dziewoński, A.M., 1985. Lower mantle heterogeneity, dynamic topography and the geoid, *Nature*, **313**, 541–545.
- Hansen, P.C., 1992. Analysis of discrete ill-posed problems by means of the L-curve, *SIAM Rev.*, **34**(4), 561–580, doi:10.1137/1034115.
- Hung, S.-H., Dahlen, F.A. & Nolet, G., 2000. Fréchet kernels for finite-frequency traveltimes—II. Examples, *Geophys. J. Int.*, **141**(1), 175–203.
- Kammann, P. & Michel, V., 2008. Time-dependent Cauchy-Navier splines and their application to seismic wave front propagation, *Z. Angew. Math. Mech.*, **88**(3), 155–178, doi:10.1002/zamm.200610362.
- Káráson, H. & van der Hilst, R.D., 2000. Constraints on mantle convection from seismic tomography, in *The History and Dynamics of Global Plate Motions*, Vol. 121: Geophysical Monograph, eds Richards, M.A., Gordon, R.G. & van der Hilst, R.D., Am. Geophys. Un., Washington, DC.
- Kellogg, O.D., 1967. *Foundations of Potential Theory*, Springer-Verlag, New York.
- Lawson, C.L. & Hanson, R.J., 1974. *Solving Least Squares Problems*, Prentice-Hall, Englewood Cliffs, NJ.
- Lévêque, J.-J., Rivera, L. & Wittlinger, G., 1993. On the use of the checkerboard test to assess the resolution of tomographic inversions, *Geophys. J. Int.*, **115**, 313–318.
- Loris, I., Nolet, G., Daubechies, I. & Dahlen, F.A., 2007. Tomographic inversion using ℓ_1 -norm regularization of wavelet coefficients, *Geophys. J. Int.*, **170**(1), 359–370, doi:10.1111/j.1365-246X.2007.03409.x.
- Mallat, S.G., 1989. Multiresolution approximations and wavelet orthonormal bases of $L^2(\mathbb{R})$, *Trans. Am. Math. Soc.*, **315**(1), 69–87.
- Masters, G. & Richards-Dinger, K., 1998. On the efficient calculation of ordinary and generalized spherical harmonics, *Geophys. J. Int.*, **135**(1), 307–309.
- Michel, V., 1999. A multiscale method for the gravimetry problem—theoretical and numerical aspects of harmonic and anharmonic modelling, *PhD thesis*, Geomathematics Group, Department of Mathematics, University of Kaiserslautern, Shaker Verlag, Aachen.
- Michel, V. & Wolf, K., 2008. Numerical aspects of a spline-based multiresolution recovery of the harmonic mass density out of gravity functionals, *Geophys. J. Int.*, **173**, 1–16, doi:10.1111/j.1365-246X.2007.03700.x.
- Montagner, J.-P., 1986. Regional three-dimensional structures using long-period surface waves, *Ann. Geophys.*, **4**(B3), 283–294.
- Müller, C., 1966. *Spherical Harmonics*, Springer-Verlag, Berlin.
- Nashed, M.Z. & Wahba, G., 1974. Convergence rates of approximate least squares solutions of linear integral and operator equations of the first kind, *Math. Comput.*, **28**(125), 69–80.
- Nashed, M.Z. & Wahba, G., 1975. Some exponentially decreasing error bounds for a numerical inversion of the Laplace transform, *J. Math. Anal. Appl.*, **52**(3), 660–668.
- Nettles, M. & Dziewoński, A.M., 2008. Radially anisotropic shear velocity structure of the upper mantle globally and beneath North America, *J. geophys. Res.*, **113**, B02303, doi:10.1029/2006JB004819.
- Nissen-Meyer, T., Dahlen, F.A. & Fournier, A., 2007. Spherical-earth Fréchet sensitivity kernels, *Geophys. J. Int.*, **168**(3), 1051–1066, doi:10.1111/j.1365-246X.2006.03123.x.
- Nolet, G., (ed.), 1987. *Seismic Tomography*, Reidel, Hingham, MA.
- Nolet, G., 2008. *A Breviary for Seismic Tomography*, Cambridge University Press, Cambridge, UK.
- Nolet, G. & Montelli, R., 2005. Optimal parametrization of tomographic models, *Geophys. J. Int.*, **161**(2), 365–372, doi:10.1111/j.1365-246X.2005.02596.x.
- Pari, G. & Peltier, W.R., 1996. The free-air gravity constraint on subcontinental mantle dynamics, *J. geophys. Res.*, **101**(B12), 28 105–28 132.
- Parker, R.L., 1994. *Geophysical Inverse Theory*, Princeton University Press, Princeton, NJ.
- Romanowicz, B., 2003. Global mantle tomography: progress status in the last 10 years, *Ann. Rev. Geoph. Space Phys.*, **31**, 303–328, doi:10.1146/annurev.earth.31.091602.113555.
- Romanowicz, B., 2008. Using seismic waves to image Earth's structure, *Nature*, **451**, 266–268, doi:10.1038/nature06583.
- Romanowicz, B. & Giardini, D., 2001. The future of permanent seismic networks, *Science*, **293**, 2000–2001.
- Saitoh, S., 2005. Best approximation, Tikhonov regularization and reproducing kernels, *Kodai Math. J.*, **28**(2), 359–367.
- Saitoh, S., Matsuura, T. & Asaduzzaman, M., 2003. Operator equations and best approximation problems in reproducing kernel Hilbert spaces, *J. Anal. Appl.*, **1**(3), 131–142.
- Sansone, G., 1959. *Orthogonal Functions (revised English edition)*, Interscience, New York.
- Schreiner, M., 1997a. Locally supported kernels for spherical spline interpolation, *J. Approx. Theory*, **89**, 172–194.
- Schreiner, M., 1997b. On a new condition of strictly positive definite functions on spheres, *Proc. Am. Math. Soc.*, **125**(2), 531–539.
- Shure, L., Parker, R.L. & Backus, G.E., 1982. Harmonic splines for geomagnetic modeling, *Phys. Earth planet. Inter.*, **28**, 215–229.
- Simons, F.J. & Dahlen, F.A., 2006. Spherical Slepian functions and the polar gap in geodesy, *Geophys. J. Int.*, **166**, 1039–1061, doi:10.1111/j.1365-246X.2006.03065.x.
- Simons, F.J., van der Hilst, R.D., Montagner, J.-P. & Zielhuis, A., 2002. Multimode Rayleigh wave inversion for heterogeneity and azimuthal anisotropy of the Australian upper mantle, *Geophys. J. Int.*, **151**(3), 738–754, doi:10.1046/j.1365-246X.2002.01787.x.
- Simons, F.J., Dahlen, F.A. & Wiecek, M.A., 2006a. Spatiospectral concentration on a sphere, *SIAM Rev.*, **48**(3), 504–536, doi:10.1137/S0036144504445765.
- Simons, F.J., Nolet, G., Babcock, J.M., Davis, R.E. & Orcutt, J.A., 2006b. A future for drifting seismic networks, *EOS, Trans. Am. geophys. Un.*, **87**(31), 305–307.
- Spakman, W. & Bijwaard, H., 2001. Optimization of cell parameterization for tomographic inverse problems, *Pure appl. Geophys.*, **158**, 1401–1423.
- Spakman, W. & Nolet, G., 1988. Imaging algorithms, accuracy and resolution in delay time tomography, in *Mathematical Geophysics: A Survey of Recent Developments in Seismology and Geodynamics*, pp. 155–187, eds Vlaar, N.J., Nolet, G., Wortel, M.J.R. & Cloetingh, S.A.P.L., Reidel, Dordrecht, The Netherlands.
- Tarantola, A. & Nercessian, A., 1984. Three-dimensional inversion without blocks, *Geophys. J. R. astr. Soc.*, **76**, 299–306.
- Tarantola, A. & Valette, B., 1982. Generalized nonlinear inverse problems solved using the least squares criterion, *Rev. Geophys.*, **20**(2), 219–232.
- Trampert, J. & Snieder, R., 1996. Model estimations biased by truncated expansions: Possible artifacts in seismic tomography, *Science*, **271**(5253), 1257–1260, doi:10.1126/science.271.5253.1257.
- Trampert, J. & Woodhouse, J.H., 1995. Global phase-velocity maps of Love and Rayleigh-waves between 40 and 150 seconds, *Geophys. J. Int.*, **122**(2), 675–690.
- Trampert, J. & Woodhouse, J.H., 1996. High resolution global phase velocity distributions, *Geophys. Res. Lett.*, **23**(1), 21–24.
- Trampert, J. & Woodhouse, J.H., 2001. Assessment of global phase velocity models, *Geophys. J. Int.*, **144**(1), 165–174, doi:10.1046/j.1365-246x.2001.00307.x.
- Trampert, J. & Woodhouse, J.H., 2003. Global anisotropic phase velocity maps for fundamental mode surface waves between 40 and 150 s, *Geophys. J. Int.*, **154**(1), 154–165, doi:10.1046/j.1365-246X.2003.01952.x.
- Tücks, M., 1996. Navier-Splines und ihre Anwendung in der Deformationsanalyse, *PhD thesis*, Geomathematics Group, Department of Mathematics, University of Kaiserslautern.
- Wang, Z. & Dahlen, F.A., 1995. Spherical-spline parameterization of three-dimensional Earth models, *Geophys. Res. Lett.*, **22**, 3099–3102.
- Wang, Z., Tromp, J. & Ekström, G., 1998. Global and regional surface-wave inversions: a spherical-spline parameterization, *Geophys. Res. Lett.*, **25**(2), 207–210.
- Wahler, K.A. & Gubbins, D., 1981. Spherical harmonic analysis of the geomagnetic field: an example of a linear inverse problem, *Geophys. J. Int.*, **65**(3), 645–693, doi:10.1111/j.1365-246X.1981.tb04877.x.

Windheuser, U., 1995. Sphärische Wavelets: Theorie und Anwendungen in der Physikalischen Geodäsie, *PhD thesis*, Geomathematics Group, Department of Mathematics, University of Kaiserslautern.

Woodhouse, J.H. & Dziewoński, A.M., 1984. Mapping the upper mantle: three-dimensional modeling of Earth structure by inversion of seismic waveforms, *J. geophys. Res.*, **89**(B7), 5953–5986.

Yanovskaya, T.B. & Ditmar, P.G., 1990. Smoothness criteria in surface wave tomography, *Geophys. J. Int.*, **102**, 63–72.

Zhang, Y.-S. & Tanimoto, T., 1993. High-resolution global upper-mantle structure and plate-tectonics, *J. geophys. Res.*, **98**(B6), 9793–9823.

Zhou, Y., Dahlen, F.A. & Nolet, G., 2004. Three-dimensional sensitivity kernels for surface wave observables, *Geophys. J. Int.*, **158**(1), 142–168.